ICASE

SPECTRAL CALCULATIONS OF

ONE-DIMENSIONAL INVISCID COMPRESSIBLE FLOWS

David Gottlieb

Liviu Lustman

and

Steven A. Orszag

Report No. 80-34

December 4, 1980

INSTITUTE FOR COMPUTER APPLICATIONS IN SCIENCE AND ENGINEERING
NASA Langley Research Center, Hampton, Virginia

Operated by the

UNIVERSITIES SPACE USRA RESEARCH ASSOCIATION

SPECTRAL CALCULATIONS OF ONE-DIMENSIONAL INVISCID COMPRESSIBLE FLOWS

David Gottlieb
Tel-Aviv University
and
Institute for Computer Applications in Science and Engineering

Liviu Lustman
Old Dominion University

Steven A. Orszag
Massachusetts Institute of Technology

ABSTRACT

The extension of spectral methods to inviscid compressible flows is considered. Techniques for high resolution treatment of shocks and contact discontinuities are introduced. Model problems that demonstrate resolution of shocks and contact discontinuities over one effective grid interval are given.

*Work was supported by the Air Force Office of Scientific Research under Grant No. 77-3405, the Office of Naval Research under Contract No. N00014-77-C-0138 and NASA Contract No. NAS1-15810 while the author was in residence at ICASE, NASA Langley Research Center, Hampton, VA 23665.

†Work was supported by Old Dominion University Grant No. NAG1-25.

‡Work was supported by the Air Force Office of Scientific Research under Grant No. 77-3405, the Los Alamos Scientific Laboratory which is supported by the Department of Energy, and the Office of Naval Research under Contract No. N00014-77-C-0138.

1. INTRODUCTION

Spectral methods [4] are based on representing the solution to a problem as a truncated series of smooth functions of the dependent variables. They have been applied to the numerical simulation of a variety of viscous flows, including the numerical simulation of turbulence [15] and the numerical simulation of transition to turbulence [14] in incompressible fluids. It may seem that spectral methods are limited to problems where Fourier series are appropriate in rectangular geometries and spherical harmonic series are appropriate in spherical geometries. In these cases, smooth solutions can be represented as rapidly converging spectral series, leading to significant economies over discrete approximations that lead to finite difference methods.

Spectral methods have now developed as a useful tool in areas far removed from their original,and perhaps obvious, applications. Transform methods [10] have allowed their application to problems with general nonlinear and nonconstant coefficients. Orthogonal polynomial expansions [4] have expanded widely the kinds of boundary conditions amenable to spectral treatment. New extensions of the fast Fourier transform to nearly arbitrary Sturm-Liouville eigenfunction bases [11] may improve the efficiency of spectral methods based on exotic function bases. A fast, general iteration method has improved the efficiency of solving general spectral equations so that spectral solution of problems in general complicated geometries requires little more work than that required to solve the lowest-order finite-difference approximation to the problem in the complex geometry [12].

One kind of problem has not yet received much attention for treatment by spectral methods, namely, the approximation of discontinuous solutions by spectral methods. Some early partial results

were encouraging. It was shown [13] that continuous solutions with discontinuous derivatives are well represented spectrally and that the accuracy advantages of spectral methods over finite difference methods survive for such solutions.

In the present paper, we provide an initial glimpse into the extension of spectral methods to treat discontinuous solutions with shocks and contact discontinuities. The results are encouraging It seems that spectral methods allow the resolution of shock fronts and contact discontinuities by shock-capturing techniques with only one grid interval across the discontinuity. Of course, spectral methods may also be used with shock-fitting techniques to represent a perfectly sharp discontinuity.

2. LINEAR HYPERBOLIC PROBLEMS

It has been shown [9] that by pre- and post- processing discontinuous data it is possible to achieve high accuracy with spectral approximations to discontinuous solutions of linear problems.

A standard model problem [1] is given by the one-dimensional wave equation

$$\frac{\partial u(x,t)}{\partial t} + \frac{\partial u(x,t)}{\partial x} = 0 \qquad (1)$$

with periodic boundary conditions on the interval $0 \leq x \leq 2\pi$. With nonsmooth initial data $u(x,0) = f(x)$, the solution $u(x,t) = f(x-t)$ (extended periodically) is nonsmooth for all t and a Fourier-spectral method should be expected to converge slowly. Nevertheless, results obtained by pseudospectral Fourier solution of [1] on a uniform grid are spectacular (at least in comparison with those obtained by such techniques as the flux-corrected transport (FCT) algorithm [1]). Of

course, both the spectral and finite-difference results may be improved using adaptive mesh-refinement methods to improve resolution near discontinuities. In Fig. 1, the solution to (1) is plotted at $t = 4\pi$ (after two full propagation periods over the spatial domain) with $f(x) = \exp(-(x-\pi)^2/4\Delta x^2)$ so the solution is a Gaussian with width $2\Delta x$, where $\Delta x = 2\pi/64$ is the effective grid resolution with 64 Fourier modes. The results plotted in Fig. 1 were obtained using a weak low-pass filter to pre- and post- process the results [see (22) below].

In Fig. 2, similar plots are given for the solution to (1) when $f(x)$ is a top-hat function. Here a stronger post-processing [see (21) below] was necessary to remove large oscillations, due to the Gibbs phenomenon, near the discontinuities. The particular post-processing does not appear to be too important for this problem; we used a one-sided average in the neighborhood of rapid changes of the solution. The motivation for this choice is similar to that of the FCT algorithm [1]. The results plotted in Figs. 1 and 2 are obtained using 64 Fourier modes, corresponding to 64 collocation points.

3. COMPRESSIBLE FLOW PROBLEMS

In this Section, we study the application of spectral methods to one-dimensional compressible flow problems. In Sec. 7, we compare the results with those obtained by more coventional finite-difference methods. The one-dimensional Eulerian equations of motion in a finite shock tube are, in conservation form,

$$\frac{\partial \vec{w}}{\partial t} + \frac{\partial}{\partial x}\vec{F}(\vec{w}) = 0 \quad (-1 \le x \le 1) \tag{2}$$

$$\vec{w} = (\rho, m, E)^T, \quad \vec{F}(\vec{w}) = u\,\vec{w} + (0, p, pu)^T \tag{3}$$

where ρ is the mass density, m is the momentum density, E is is the total energy density, p is the pressure and $u = m/\rho$ is the velocity.

We assume the equation of state to be

$$p = (\gamma-1)\left[E - \frac{1}{2}\rho u^2\right]; \tag{4}$$

usually, we take $\gamma = 1.4$, as is appropriate for a diatomic gas.

For simple shock tube problems, that involve only constant states separated by shocks and contact discontinuities, there is no immediate need for high-order accurate numerical methods. However, for more complicated flow problems, especially in higher dimensions, where there may be interacting shocks, rarefaction waves, contact discontinuities as well as the interaction of shocks with boundary layers and interfaces, it is necessary to have both high accuracy in the interior of the flow, in the boundary layers, near the interfaces, as well as good representations of discontinuities. From this point of view it seems appropriate to use the Chebyshev spectral method since it provides both high interior accuracy and very high resolution in the boundary layer region [4].

We regard the classical simple shock tube problems as extremely severe tests of spectral methods. After all, spectral methods are designed to give good resolution of complicated flow structures distributed through the flow domain and, since they are based on expansions in orthogonal functions, it would seem that isolated local jumps at shocks and contact discontinuities would be most inhospitable for them. On the other hand, it would seem that low-order finite-difference methods would be best for treating shock discontinuities because of their localized character. One of the important conclusions of this paper is that the accuracy (or rather,

the resolution) advantages of spectral methods hold up in the neighborhood of shock discontinuities, not just in regions of smooth flows and boundary layers.

There are three ways to apply Chebyshev-spectral methods to these problems, namely, collocation, Galerkin, and tau approximations [4]. We choose to use the collocation (or pseudospectral) technique here for two reasons. First, collocation is the easiest and most efficient method to apply for complicated problems. Also, since collocation involves solving the equations in physical space rather than in transform space with transforms used only to evaluate derivatives, boundary conditions are also easier to apply.

Let us give a brief description of the collocation method. At each time step, we evaluate the components of $\vec{F}$ in (2) at the points

$$x_j = \cos \pi j/N \quad (0 \le j \le N) \tag{5}$$

Next, the Chebyshev expansion coefficients $\vec{a}_n$ of $\vec{F}$ are found from

$$\vec{F}(x_j) = \sum_{n=0}^{N} \vec{a}_n T_n(x_j) \quad (0 \le j \le N), \tag{6}$$

where $T_n(x)$ is the Chebyshev polynomial of degree n defined by $T_n(x) = \cos(n \cos^{-1} x)$. Since $T_n(x_j) = \cos \frac{\pi jn}{N}$ it follows that

$$\vec{a}_n = \frac{2}{N\bar{c}_n} \sum_{n=0}^{N} \frac{1}{\bar{c}_p} \vec{F}(x_p) \cos \frac{\pi pn}{N} \quad (0 \le n \le N) \tag{7}$$

where $\bar{c}_o = \bar{c}_N = 2$, and $\bar{c}_n = 1$ for $0 < n < N$. Differentiating (6) gives

$$\frac{\partial \vec{F}}{\partial x} = \sum_{n=0}^{N} \vec{a}_n T_n' = \sum_{n=0}^{N} \vec{s}_n T_n \tag{8}$$

where

$$\vec{s}_n = \frac{2}{\bar{c}_n} \sum_{\substack{p=n+1 \\ p+n \text{ odd}}}^{N} p\vec{a}_p. \tag{9}$$

Eqs. (7) - (8) are implemented using the fast Fourier transform. In order to avoid having to perform order N^2 operations to evaluate (9) we observe that $\vec{s}_N = 0, \vec{s}_{N-1} = 2N\vec{a}_N$ and $\vec{s}_n (n \leq N-2)$ satisfies the recurrence relation

$$\vec{c}_n \vec{s}_n = \vec{s}_{n+2} + 2(n+1)\vec{a}_{n+1} \quad (n \leq N-2) \tag{10}$$

Using (10), only $0(N)$ operations are necessary to obtain $\vec{s}_n$ from $\vec{a}_n$. Thus, using the fast Fourier transform, evaluation of $\partial \vec{F}/\partial x$ from $\vec{F}$ requires only order $N \log N$ operations.

It should be noted that the collocation points x_j are crowded in the neighborhood of $x = 1$, and $x = -1$. [x_1 and x_{N-1} are located at distances of $\pi^2/2N^2$ from $x = 1, -1$, respectively]. For $N = 128$, there are 40 points located in the interval $0.9 < |x| \leq 1$. This high boundary resolution can be of great value when boundary layers or interfaces are also present, but is wasteful for the simple test problems of the present paper.

Next, we describe some time marching techniques. Let us denote the discrete approximation for $\vec{w}$ at collocation point x_j and time step $n\Delta t$ by $\vec{w}_j^n$ the discrete approximation for $\vec{F}$ by $\vec{F}_j^n$. Then we advance in time using the two-step (modified Euler) method

$$\vec{w}_j^{\,n+\frac{1}{2}} = \vec{w}_j^{\,n} - \frac{1}{2}\Delta t\left(\frac{\partial \vec{F}}{\partial x}\right)_j^n \tag{11}$$

$$\vec{w}_j^{\,n+1} = \vec{w}_j^{\,n} - \Delta t\left(\frac{\partial \vec{F}}{\partial x}\right)_j^{n+\frac{1}{2}} \tag{12}$$

This scheme results in a linear stability condition of the form

$$\Delta t \leq \frac{8}{N^2 \max(|u|+c)} \tag{13}$$

where c is the sound speed. This condition is very severe; indeed, using finite difference methods with N points leads to stability restrictions like $\Delta t = O(1/N)$. An alternative approach is given in [5] and [12] that avoids the latter difficulty. The approach described in [5] yields an unconditionally explicit stable scheme whereas that described in [12] involves a very efficient implicit technique.

In this paper, however, we present results gotten by using (11) (12). Application of the other time marching techniques will be given elsewhere.

4. CONSERVATION PROPERTIES OF PSEUDOSPECTRAL METHODS

In this Section we discuss the conservation properties of pseudospectral methods applied to a nonlinear system of equations. Consider the

$$\frac{\partial \vec{w}}{\partial t} = \frac{\partial \vec{F}(\vec{w})}{\partial x}$$

$$\vec{w}(x,0) = \vec{\phi}(x) \tag{14}$$

It is well known that, in general, no smooth solution can exist for all time. Instead one seeks a weak solution defined by the requirement that the integral relation

$$\int\int(\vec{\psi}_t w - \psi_x \vec{F})\,dx\,dt + \int \vec{\psi}(x,0)\vec{\phi}(x) = 0 \qquad (15)$$

be satisfied for all smooth test vectors $\vec{\psi}$ which vanish both for large t and on the boundary of the domain.

It can be shown that as a result of the integral relation (14) the weak solution must satisfy the Rankine-Hugoniot shock conditions. Assume now that (14) is spatially discretized by the pseudospectral Fourier method (see [4]). By this we mean that $\vec{w}_N(x,t)$ is defined as the trigonometric interpolant of $\vec{w}(x,t)$ at the points $x = \frac{\pi j}{N+1}$ $(j = 0, \ldots, 2N)$, $\vec{F}_N(x,t)$ is defined as the interpolant of $\vec{F}$ at x_j, and one solves the $2N + 1$ vector equations

$$\frac{\partial \vec{w}_N}{\partial t}(x,t) = \frac{\partial \vec{F}_N}{\partial x}(x_j,t) \quad (j = 0,\ldots,2N) \qquad (16)$$

This discretization should be used only if the boundary conditions of (14) are periodic with period 2π.

Following Lax and Wendroff [8] we can prove

Theorem 1: Assume that as $N \to \infty$, $\vec{w}_N$ converges boundedly to some vector $\vec{w}$. Then $\vec{w}(x,t)$ is a weak solution of (14) with initial value $\vec{\phi}$.

Proof: Let $\vec{\psi}(x,t)$ be a periodic test function and let $\vec{\psi}_N(x,t)$ be the interpolant of $\vec{\psi}$ at $x = x_j$. Let $\vec{\phi}_N(x)$ be the interpolant of ϕ at the same points.

Multiplying (16) by $\psi_N(x_j)$ and summing one gets

$$\sum_{j=0}^{2N} \vec{\psi}_N(x_j)\,\frac{\partial \vec{w}_N}{\partial t}(x_j,t) = \sum_{j=0}^{2N} \vec{\psi}_N(x_j)\,\frac{\partial \vec{F}_N(\vec{w}_N(x_j,t))}{\partial x}.$$

We interpret now the sums on both sides of this result in terms of the trapezoidal integration rule. Since $\psi_N w_N$ and $\psi_N F_N$ are trigonometric polynomials of degree $2N$, the trapezoidal rule is exact (see [2]). Therefore, we obtain

$$\int_0^{2\pi} \psi_N(x,t)\, \frac{\partial \vec{w}_N}{\partial t}(x,t)\,dx = \int_0^{2\pi} \vec{\psi}_N(x,t) \frac{\partial \vec{F}_N}{\partial x}(x,t)\,dx = -\int_0^{2\pi} \vec{F}_N(x,t)\, \frac{\partial \vec{\psi}_N}{\partial x}$$

We integrate now with respect to t to get

$$\int_0^{2\pi} dx \int_0^{\infty} dt\, \vec{\psi}_N(x,t)\, \frac{\partial \vec{w}_N}{\partial t}(x,t) + \int_0^{\infty} dt \int_0^{2\pi} dx\, \vec{F}_N(x,t)\, \frac{\partial \vec{\psi}_N}{\partial x} = 0$$

Integrating the left hand side by parts and taking into account that $\psi_N(x,t) \to 0 \quad t \to \infty$ we obtain

$$-\int_0^{2\pi} \vec{\psi}_N(x,0)\vec{w}_N(x,0)\,dx - \int_0^{2\pi} \int_0^{\infty} [\vec{w}_N(x,t)\, \frac{\partial \vec{\psi}_N}{\partial t}(x,t) - \vec{F}_N(x,t) \frac{\partial \vec{\psi}_N}{\partial x}(x,t)]\,dx\,dt = 0$$

or

$$\int_0^{2\pi} \vec{\psi}_N(x,0)\vec{\phi}_N(x) + \int_0^{2\pi} \int_0^{\infty} [\vec{w}_N(x,t)\, \frac{\partial \vec{\psi}_N}{\partial t}(x,t) - \vec{F}_N(x,t)\, \frac{\partial \vec{\psi}_N}{\partial x}(x,t)]\,dx\,dt = 0$$

Letting $N \to \infty$ completes the proof of the Theorem.

Theorem 1 establishes the fact that the pseudospectral Fourier method applied to problems with shocks yields the correct shock speed. The following argument [7] asserts that this method can achieve resolution of shock discontinuities over 1 effective grid interval. If the numerical approximation u_{ap} to an exact shock solution u_{ex} over the interval $0 \le x < 2\pi$ is smeared over a distance h near a shock of strength U then

$$\int_0^{2\pi} (u_{ex} - u_{ap})^2\, dx \gtrsim \frac{1}{3} h U^2$$

where the constant $\frac{1}{3}$ obtains if the error $u_{ex} - u_{ap}$ varies linearly from 0 to U over a distance $\frac{1}{2}h$. On the other hand, it is, in principle, possible that the first N Fourier coefficients of u_{ap} in an N term Fourier spectral calculation agree closely with those

of u_{ex}. Since the nth Fourier coefficient a_n of a shock solution on $[0,2\pi]$ behaves asymptotically as $U/2\pi n$ as $n \to \infty$, it follows that

$$\int_0^{2\pi} (u_{ex} - u_{ap})^2 \, dx \leq 2\pi \sum_{|n|>\frac{N}{2}} |a_n|^2 \sim \frac{2U^2}{\pi N}$$

Therefore,

$$h \leq \frac{6}{\pi N}$$

Since the effective grid separation Δ is $2\pi/N$, it follows that, optimally,

$$h \leq \frac{1}{3} \Delta$$

or better than 1 grid interval resolution.

It is interesting to note that (16) implies that the component of $\vec{w}_N$ are conserved. In fact, summing up both sides of (16) one gets

$$\sum_{j=0}^{2N} \frac{\partial \vec{w}_N}{\partial t}(x_j,t) = \sum_{j=0}^{2N} \frac{\partial \vec{F}_N}{\partial x}(x_j,t)$$

By the same argument as before one can replace the sums by integrals to get

$$\frac{d}{dt} \int_0^{2\pi} w_N(x,t) \, dx = \int_0^{2\pi} \frac{\partial \vec{F}_N}{\partial x}(x,t) \, dx = 0$$

Therefore

$$\int_0^{2\pi} \vec{w}_N(x,t)dx = \int_0^{2\pi} \vec{w}_N(x,0)dx.$$

For compressible flow problems, this shows that the mass, momentum, and energy are conserved.

We would like now to demonstrate that the same conservation properties that were established for the pseudospectral Fourier method hold also for the pseudospectral Chebyshev method. In analogy to Theorem 1 we can prove :

Theorem 2: Let $\vec{w}_N$ and $\vec{F}_N$ be the pseudospectral Chebyshev approximation described in (5) - (10) to equation (14). Then if $\vec{w}_N$ converges to $\vec{w}$ and $\vec{\psi}$ is a smooth test function such that $\vec{\psi}(-1,t) = \vec{\psi}(1,t) = 0$ $\vec{\psi}(x,\infty) = 0$ then $\vec{w}(x,t)$ is a weak solution of (14).

Proof: It is shown in [4, p. 15] that $\vec{w}_N$ satisfies exactly the equation

$$\frac{\partial \vec{w}_N}{\partial t} = \frac{\partial \vec{F}_N}{\partial x} + \vec{\tau}(t)\, U_{N-1}(x) P(x) \qquad (17)$$

where U_{N-1} is the Chebyshev polynomial of the second kind so that $U_{N-1}(x_j)=0$ for $j = 1,\ldots,N-1$ and $P(x)$ is a polynomial of degree 1 that corresponds to the boundary condition. More precisely, $P(x) = 1-x$ when the boundary data is prescribed at $x =-1$ and $P(x) = 1+x$ when the boundary data is prescribed at $x = +1$. Suppose $\vec{\psi}_{N-3}$ is the interpolant of $\vec{\psi}/\sqrt{1-x^2}$ at the points $y_j = \cos\frac{\pi j}{N-3}$ $(j = 0,\ldots,N-3)$ then

$$\int_{-1}^{1} \sqrt{1-x^2}\, \vec{\psi}_{N-3}\, \frac{\partial \vec{w}_N}{\partial t}\,(x,t) = \int_{-1}^{1} \sqrt{1-x^2}\, \vec{\psi}_{N-3} \frac{\partial \vec{F}_N}{\partial x} + \vec{\tau} \int_{-1}^{1} U_{N-1} P(x) \vec{\psi}_{N-3} \sqrt{1-x^2}\, dx$$

(18)

Since $P(x)\vec{\psi}_{N-3}(x)$ is a polynomial of degree $N-2$ the last integral at the right hand side of (18) vanishes.

The rest of the proof is similar to the proof of Theorem 1. Defining

$$\vec{\rho}_N = \sqrt{1-x^2}\,\vec{\psi}_{N-3}$$

and integrating we obtain

$$\int_{-1}^{1} \vec{w}_N(x,0)\vec{\rho}_N(x,0)dx + \int_0^{\infty}\int_{-1}^{1} (\vec{w}_N \frac{\partial \vec{\rho}_N}{\partial t} - \vec{F}_N \frac{\partial \vec{\rho}_N}{\partial x})\, dx\, dt = 0$$

Since $\vec{\rho}_N \to \vec{\psi}$ uniformly and the derivatives of $\vec{\rho}_N$ converge similarly to the derivatives of $\vec{\psi}$, and since $\vec{w}_N \to \vec{w}$, the proof is completed.

We are also able to show that the components of $\vec{w}$ are conserved. In fact since

$$\frac{\partial \vec{w}_N}{\partial t}(x_j) = \frac{\partial \vec{F}_N}{\partial x}(x_j) \qquad (19)$$

for all interior points x_j, one can use the Clenshaw-Curtiss quadrature formula [2] to get

$$\sum_{j=0}^{N} \frac{\partial w_N}{\partial t}(x_j)\alpha_j = \int_{-1}^{1} \frac{\partial w_N}{\partial t}\, dx$$

$$\sum_{j=0}^{N} \frac{\partial F_N}{\partial x}(x_j)\alpha_j = \int_{-1}^{1} \frac{\partial F_N}{\partial x}\, dx - F_N(1) - F_N(-1)$$

where

$$\alpha_j = \alpha_{N-j} = \frac{4}{N} \sum_{k=0}^{N/2} \frac{1}{1-4k^2} \cos \frac{\pi jk}{N}$$

$$\alpha_0 = \alpha_N = \frac{1}{N^2-1}$$

Therefore (19) gives

$$\frac{d}{dt} \int_{-1}^{1} \vec{w}_N \, dx = \vec{\sigma}$$

where $\vec{\sigma}$ represents the contribution from the boundaries. In the case of homogeneous boundary conditions where $\vec{w}_N$ and $\partial \vec{F}_N / \partial x$, $\vec{\sigma} = 0$ so that both vanish at the boundaries.

$$\int_{-1}^{1} \vec{w}_N(x,t) \, dx = \int_{-1}^{1} \vec{w}_N(x,0) \, dx, \tag{20}$$

demonstrating conservation.

5. BOUNDARY CONDITIONS

Boundary conditions play a crucial role in the application of spectral methods. Incorrect boundary treatment may give strong instabilities, in contrast to finite difference methods in which instabilities due to boundaries usually appear as relatively weak oscillations. On the other hand, as opposed to high-order finite-difference methods, spectral methods normally do not require numerical boundary conditions in addition to the physical boundary conditions required by the partial differential equation.

For shock tube problems, we must specify all the flow variables at supersonic inflow points, two flow variables at subsonic inflow points, and one flow variable at subsonic outflow points. If we over-specify or underspecify the boundary conditions, spectral calculations are usually spectacularly unstable.

At subsonic outflow points, it is not satisfactory to specify arbitrarily any one of the flow variables m, ρ, u or E. With arbitrary outflow boundary conditions, one can obtain oscillations that originate

at the boundary. The outflow boundary conditions used here were obtained following the analysis given in [3] . We advance one time step without imposing the boundary conditions and denote the calculated quantities by $\vec{w}_c$. We observe that if $x = +1$ is a subsonic outflow point, the incoming characteristic quantity at $x = +1$ is

$$v_1 = p - (\rho c)\, u$$

whereas the outgoing characteristic quantities are

$$v_2 = p + (\rho c)\, u, \quad v_3 = p - c^2 \rho.$$

Let us assume that one flow variable is given on the inflow characteristic at $x = +1$. Then we solve the system

$$v_2 = (v_2)_c, \quad v_3 = (v_3)_c \tag{21}$$

for the two remaining flow variables at $x = 1$. This procedure yields a stable scheme with no oscillations emanating from the boundaries. In contrast to inflow-outflow boundaries whose treatment is quite systematic by the above procedure, material boundaries evidently do require boundary conditions in addition to those required by the mathematical theory of characteristic initial value problems. At characteristic surfaces, like material boundaries, the specification of one flow variable, like $u = 0$, should suffice. However, we find that it is necessary to supplement this boundary condition at only one characteristic boundary by one additional condition, like p given. An analysis of these boundary conditions will be given elsewhere.

6. SMOOTHING AND FILTERING

The approximation of discontinuous functions by truncated Chebyshev polynomial expansions exhibits the Gibbs phenomenon near jumps and has two point oscillations over the whole region [4] . Similar oscillations are observed when approximating shock waves in inviscid flows. These oscillations may induce instabilities in nonlinear problems since they can interact with the smooth part of the solution and be amplified. It is essential for stability reasons either to eliminate completely these oscillations or to control them in such a way that stability is not affected.

Several methods to achieve stable computations have been investigated including artificial viscosity, Shuman filtering, and a new spectral filtering method to be described below. We will report results obtained by the latter two methods.

Shuman filtering involves applying the filter

$$\bar{w}_j^n = w_j^n + \theta_{j+\frac{1}{2}} (w_{j+1}^n - w_j^n) + \theta_{j-\frac{1}{2}} (w_j^n - w_{j-1}^n). \tag{22}$$

The idea is to choose smoothing factors θ_j that vanish in smooth parts of the solution and become large only in the neighborhood of discontinuities. Following Harten and Tal-Ezer [6] we choose

$$\theta_{j+\frac{1}{2}} = \beta \frac{|\rho_{j+2} - \rho_{j+1} - 2(\rho_{j+1} - \rho_j) + (\rho_j - \rho_{j-1})|}{|\rho_{j+2} - \rho_{j+1}| + 2|\rho_{j+1} - \rho_j| + |\rho_j - \rho_{j-1}|} \tag{23}$$

where $0 < \beta < 1$ is a suitable constant. Typically $\beta = 0.01$ in our calculations.

A more intriguing kind of filtering is based on the following idea. If a low-pass spectral filter just strong enough to remove those high frequency waves that lead to numerical instabilities is applied to the inviscid compressible flow equations, the spectral

equations will give bad oscillations near shock fronts and other discontinuities. However, as recently pointed out by Lax [7], these oscillatory solutions obtained by a high-order method like a spectral method should contain enough information to be able to reconstruct the proper nonoscillatory discontinuous solution by a post-processing filter. The idea is that very weak filtering or damping to stabilize together with a final 'cosmetic' filter to present the results should be able to give great improvements in resolution.

In practice, we use a low-pass filter for stabilizing purposes that is of the form

$$f(k) = \begin{cases} 1 & k < k_0 \\ e^{-\alpha (k-k_0)^4} & k > k_0 \end{cases} \tag{24}$$

where k is a spectral (wavenumber) index, k_0 depends on the strength of the shock and α is a constant of order 1. For typical fluid dynamical shocks, we choose $k_0 \sim \frac{5}{6} N$ where N is the maximum wavenumber in the spectral represention of the flow. We have found that, for moderate shocks, the results are insensitive to the detailed form of (24). However, it is important that $f(k)$ be low-pass so $f(k) = 1$ for $k < k_0$, in order that large-scales be treated very accurately (without phase error) by the spectral method.

Finally, we explain how to post-process the numerical results to retrieve smoothed results with localized discontinuities from the noisy, but stable, calculations. Our method is to first determine the location of the discontinuities in the flow and then to apply a Shuman filter to smooth the data on either side of the discontinuities (without using data from the opposite side of the discontinuity in the smoothing process). The key to the success of this procedure is the apparent ability of the spectral results to preserve information on

the precise location of discontinuities. Similar post-processing methods do not work so well on finite-difference results because, in such calculations, the shock position does not seem to be localized with one grid interval.

The location of discontinuities is found by an examination of the spectral coefficients. One may assume that the smooth part of the solution is well represented by the first few coefficients, while the leading behavior of the high-order coefficients is generated by the discontinuities. As a rule of thumb, we examine the middle third of the coefficients, since the highest third may be unreliable due to the stabilizing smoothing.

The expansion coefficients a_k should be fit by an expression of the form:

$$a_k = \sum_{s=1}^{S} B_s \, A_k(X_s) \qquad \frac{N}{3} \leq k \leq \frac{2N}{3} \tag{25}$$

where S is the number of shocks, $A_k(X)$ is the spectral coefficient of a Heaviside function with a jump at X and B_s, X_s are the intensities and locations, respectively, of the various shocks.

In our case (Chebyshev collocation) it may be readily verified that

$$A_k(X) = \frac{1}{N} \frac{\sin \frac{k\pi}{N}(L+1/2)}{\sin \frac{k\pi}{2N}} \qquad (0<k<N) \tag{26}$$

$$A_0(X) = \frac{L+1/2}{N}$$

$$A_N(X) = \frac{1}{2N} \sin \pi (L + \tfrac{1}{2})$$

with L an integer related to X by:

$$\cos \frac{(L+1)\pi}{N} < X < \cos \frac{L\pi}{N} \tag{27}$$

The solution of (25) for B_s, X_s proceeds as follows: First we rewrite (25) in the form:

$$Na_k \sin \frac{k\pi}{2N} \overset{\text{def}}{\equiv} \tilde{a}_k = \sum_{s=1}^{S} B_s \sin(k\omega_s)$$

with

$$\omega_s = (L(X_s) + \frac{1}{2}) \frac{\pi}{N}$$

Now remark that a sequence

$$b_k = \sin k\omega$$

satisfies the identity:

$$\frac{b_{k-1} + b_{k+1}}{2} \overset{\text{def}}{\equiv} (\Omega b)_k = \cos \omega \, b_k$$

Therefore, the values ω_s are simply related to the eigenvalues of the summation operator Ω. They may be computed independently of B_s; the jump magnitudes are found after the ω_s are determined, by a least squares procedure.

We applied this algorithm to the test case of several Heaviside functions added to a smooth background, such as e^x. Shock locations are recovered exactly They are assigned to the nearest "midpoint" by (27). With $N = 64$, the predicted shock intensities are correct within a few percent, for as many as 7 shocks. Moreover, when more shocks are sought than are actually present, some ω_s become imaginary, which serves as a useful check.

When actual computational data are input to the "shock locator" program described above, several jumps may be identified (of course, with the number of shocks not specified beforehand). One may then proceed in different ways:

a) Smooth between the shock locations, using one sided smoothing at the shocks.

b) Subtract the sum of Heaviside functions and smooth the result in physical space (e.g., using a Shuman filter)

c) Subtract the coefficients of the Heaviside functions found, and smooth in the coefficient space (e.g., by deleting high order coefficients).

Of these, method (a) seems the most robust as it needs no values for the actual shock intensities. In computer experients, all three methods perform comparably.

There are many fine adjustments that have to be made on the general algorithm to obtain the best results. On mildly oscillating data, one may obtain spurious shocks due to large differences from 'point to point'; sometimes, since several such oscillations are interpreted as shocks the algorithms errs simply because S is too large. We are investigating some ways of avoiding spurious shocks, namely, imposing an entropy condition, ignoring shocks of low intensity, weighting the coefficients or data, and iterating the smoothing procedure. There is not yet an approach which will solve all hard problems, although reasonably good results are not hard to obtain.

7. NUMERICAL RESULTS

The first model problem is a shock tube problem with a diatomic gas ($\gamma = 1.4$) satisfying supersonic inflow at $x = -1$ and subsonic outflow at $x = +1$. The initial conditions are

$$p = \rho_1,\ \rho = \rho_1,\quad u = u_1 \quad (-1 < x \leq 1), \tag{28}$$

while the conditions applied at the inflow point $x = -1$ are

$$p = p_2,\ \rho = r(\xi,\rho_1),\quad u = \bar{u}(\xi,\rho_1,p_1,u_1) \tag{29}$$

where

$$r(\xi,\rho_1)=\frac{1+6\xi}{\xi+6}\ \rho_1, \bar{u}(\xi,\rho_1,p_1,u_1) = u_1 - 5\ \frac{(\xi-1)}{\sqrt{42\xi+7}}\sqrt{\frac{p_1}{\rho_1}} \tag{30}$$

and $\xi = P_2/P_1$ is the strength of resulting shock. With these initial and boundary conditions, a pure shock propagates from $x = -1$ toward $x = +1$ at a speed

$$v_s = u_1 + \sqrt{\frac{p_1+6p_2}{7\rho_1}} \tag{31}$$

In Fig. 3, we plot the density structure of the resulting shock wave at $t = 0.1$ determined by the Chebyshev spectral method with $N = 64$ polynomials, $\xi = 5$ in (28) - (31), and $P_1 = \rho_1 = U_1 = 1$. The exact pressure jump across this shock wave is 5 and the density jump is 2.81818. The shock speed is 3.48997. In these calculations the low-pass filter (24) is applied every time step and the final results are cosmetically filtered by a one-sided Shuman filter (22) with constant θ_j, replaced by one-sided smoothing at shocks. Also, we plot in Fig. 3 the results obtained using a localized Shuman filter (22) with (23) at every time step. The latter result is similar to results obtained using a von Neumann-Richtmyer artificial viscosity. Observe that the cosmetically filtered results yield a one-point shock while the localized Shuman filter yields a three-point shock. Similar results are obtained applying the localized Shuman filter only every 100 steps or so.

In Fig. 4, we give a similar plot of the density across a strong shock with $\xi = 10^4$ at $t = 0.005$. Here the density jump is 5.9965. The results ploted in Figs. 3,4 demonstrate that our methods achieve high resolution shocks without significant oscillations.

The second model problem is a shock tube problem with $x = \pm 1$ as material boundaries. The initial conditions at $t = 0$ are:

$$p = \begin{cases} 1.0 & x < 0 \\ 0.55 & x = 0 \\ 0.1 & x > 0 \end{cases} \qquad (32)$$

$$\rho = \begin{cases} 1.0 & x < 0 \\ 0.5625 & x = 0 \\ 0.125 & x > 0 \end{cases}$$

$$u = 0$$

while the boundary conditions are

$$u = 0 \quad x \pm 1$$
$$\rho = 1 \quad x = -1 \qquad (33)$$

For moderate t, the solution to this problem consists of one shock, one contact discontinuity and a rarefaction wave.

A variety of difference methods for solution of the flow that evolves from (32) - (33) have been compared by Sod [16]. We have solved this problem using the spectral filtering method with $N = 64$ Chebyshev polynomials to represent the flow (in contrast to Sod's

100 point grid). The results are plotted in Fig. 5 at $t = 0.3$. Both the shock and contact discontinuity are resolved over only one grid point. The overall solution is in good agreement with the exact solution to the problem. However, without the 'cosmetic' final filter, the results are highly oscillatory. Evidently, the highly oscillatory, but stable, spectral solutions do contain enough information to reconstruct sharp discontinuities.

Finally, we consider a problem in which we test for possible degreading of the solution due to the nonlinear interaction between oscillations arising from interacting shock waves. The initial conditions are

$$p = \rho = u = 1, \quad -0.9 < x \leq 1$$

$$p = 2, \ \rho = r(2,1), \quad u = \bar{u}(2,1,1,1), \quad -1 < x \leq -0.9 \tag{34}$$

$$p = 5, \ \rho = r(2.5, r(2,1)), \ u = \bar{u}(2.5, r(2,1)), \ 2, \bar{u}(2,1,1,1)), \quad x = -1$$

These initial conditions correspond to a $\xi = 2.5$ shock lying a distance 0.1 behind a $\xi = 2$ shock. The stronger shock overtakes the weaker shock and generates a single coalesced shock and associated contact discontinuities and rarefaction wave. The resulting density at $t = 0.4$ after shock coalescence is plotted in Fig. 6. Observe that the cosmetic filtering method gives good resoluton of both the shock and the contact discontinuity while the localized Shuman filtering method deteriorates in the neighborhood of the contact.

In conclusion, we believe that the excellent results achieved by the present initial investigation of spectral methods for highly compressible flows suggests that these methods may prove useful for problems of practical interest. Such applications are now underway.

REFERENCES

1. Boris, J. P. and Book, D. L., Solution of Continuity Equations by the Method of Flux-Corrected Transport, Methods in Computational Physics, Academic, Vol. 16, Chap. 11 (1976).
2. Davis, P. J. and Rabinowitz, P., Methods of Numerical Integration, Academic (1975).
3. Gottlieb, D., Gunzburger, M., and Turkel, E., On Numerical Boundary Treatment for Hyperbolic Systems, SIAM J. Num. Anal., in press (1980).
4. Gottlieb, D. and Orszag, S. A., Numerical Analysis of Spectral Methods: Theory and Applications, NSF-CBMS Monograph No. 26, Soc. Ind. Appl. Math. Philadelphia, (1977).
5. Gottlieb, D. and Turkel, E., On Time Discretizations for Spectral Methods, Stud. in Appl. Math., in press. (1980).
6. Harten, A. and Tal-Ezer, H., On a Fourth Order Accurate Implicit Finite Difference Scheme for Hyperbolic Conservation Laws, to be published (1980).
7. Lax, P. D., Accuracy and Resolution in the Computation of Solutions of Linear and Nonlinear Equations, Recent Adv. Num. Anal., Proc. Symp. Mathematics Research Center (Univ. of Wisconsin), Academic, New York, 1978, pp. 107-117.
8. Lax, P. D. and Wendroff, B., Systems of Conservation Laws, Comm. Pure Appl. Math. 23 (1960), pp. 217-237.
9. Majda, A. McDonough, J. and Osher, S., The Fourier Method for Nonsmooth Initial Data, Math. Comp. 32 (1978) pp. 1041-1081.

10. Orszag, S. A., Numerical Simulation of Incompressible Flows Within Simple Boundaries: I. Galerkin (Spectral) Representations, Stud. in Appl. Math. 50 (1971), pp. 293-327.

11. Orszag, S. A., 'Fast'Eigenfunction Transforms, to be published (1980).

12. Orszag, S. A., Spectral Methods for Problems in Complex Geometries, J. Comp. Phys.,37 (1980), pp. 70-92 .

13. Orszag, S. A., and Jayne, L. W., Local Errors of Difference Approximations to Hyperbolic Equations, J. Comp. Phys. 14, (1974), pp. 93-103.

14. Orszag, S. A. and Patera, A. T., Subcritical Transition to Turbulence in Plane Channel Flows, Phys. Rev. Letters 45 (1980), pp. 989-993.

15. Orszag, S. A. and Patterson, G. S., Numerical Simulation of Three-Dimensional Homogeneous Isotropic Turbulence, Phys. Rev. Letters 28 (1972), pp. 76-79.

16. Sod, G. A., A Survey of Several Finite Difference Methods for Systems of Nonlinear Hyperbolic Conservation Laws, J. Comp. Phys. 27 (1978), pp. 1-31.

FIGURE CAPTIONS

Figure 1. A plot of the solution to the wave equation (1) with $f(x) = \exp(-(x-\pi)^2/4\Delta x^2)$ at $t = 4\pi$ when the initial pulse has been transported two full periods. A Fourier spectral method with $N = 64$ modes and a weak low-pass filter was used. The plotted results are in excellent agreement with the exact solution $f(x-t)$.

Figure 2. Same as Fig. 1 except $f(x) = 1(|x-\pi| < \frac{1}{2}\pi)$, $0(|x-\pi| > \frac{1}{2}\pi)$. Here a one-sided average was used as a post-filter to remove the oscillations. Again the plotted results at $t = 4\pi$ are in excellent agreement with the exact solution $f(x-t)$.

Figure 3. A plot of the density ρ vs x for the shock tube problem with initial conditions (28) - (29) with shock strength $\xi = 5$. at $t = 0.1$ obtained using the pseudospectral method with $N = 64$ Chebyshev polynomials. (a) Results obtained applying the low-pass filter (24) at every time step. (b) Results obtained by applying the post-processing Shuman filter (22) with constant θ_j [except one-sided at the shock] to the results plotted in (a). (c) Results obtained using a Shuman filter (22) with (23) [with no low-pass filter] at every time step.

Figure 4. Same as Figure 3 except $\xi = 10^4$, $t = 0.005$.

Figure 5. Plots of the density, pressure, velocity, and energy at $t = 0.3$ for the shock tube problem with initial-boundary conditions (32)-(33). The Chebyshev spectral equations were truncated at $N = 64$ polynomials and the spectral filtering method was applied to smooth the final results.

Figure 6. A plot of the density ρ vs x for the two-shock problem with initial conditions (34). Here a $\xi = 2.5$ shock lies initially a distance 0.1 behind a $\xi = 2$ shock. The density is plotted at $t = 0.4$, after shock coalescence. (a) Low-pass filter (24) only. (b) Post-processing filter (22) with constant θ_j [except one-sided at calculated discontinuities] applied to the results of (a). (c) Shuman filter (22) with (23) at every time step.

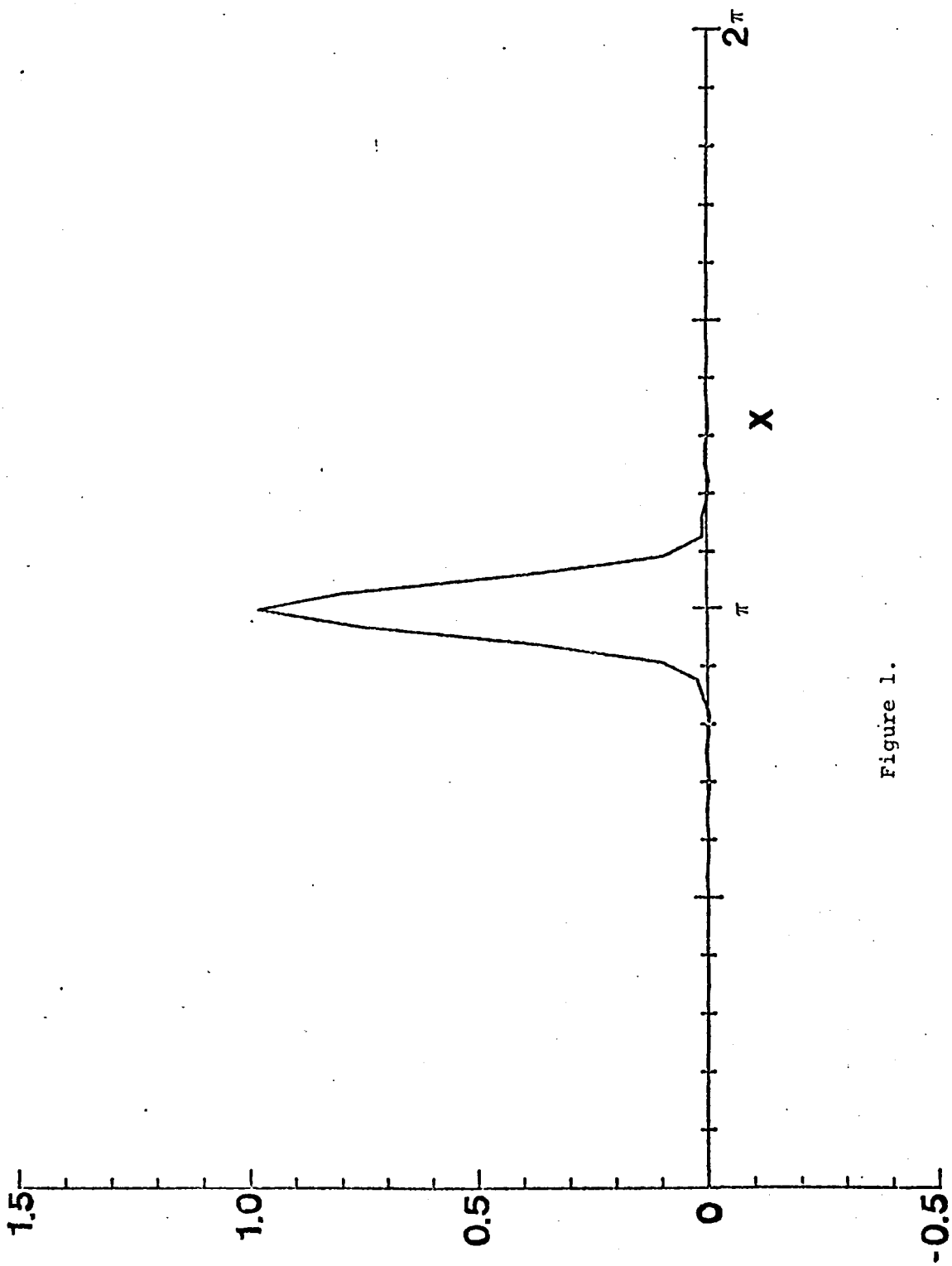

Figure 1.

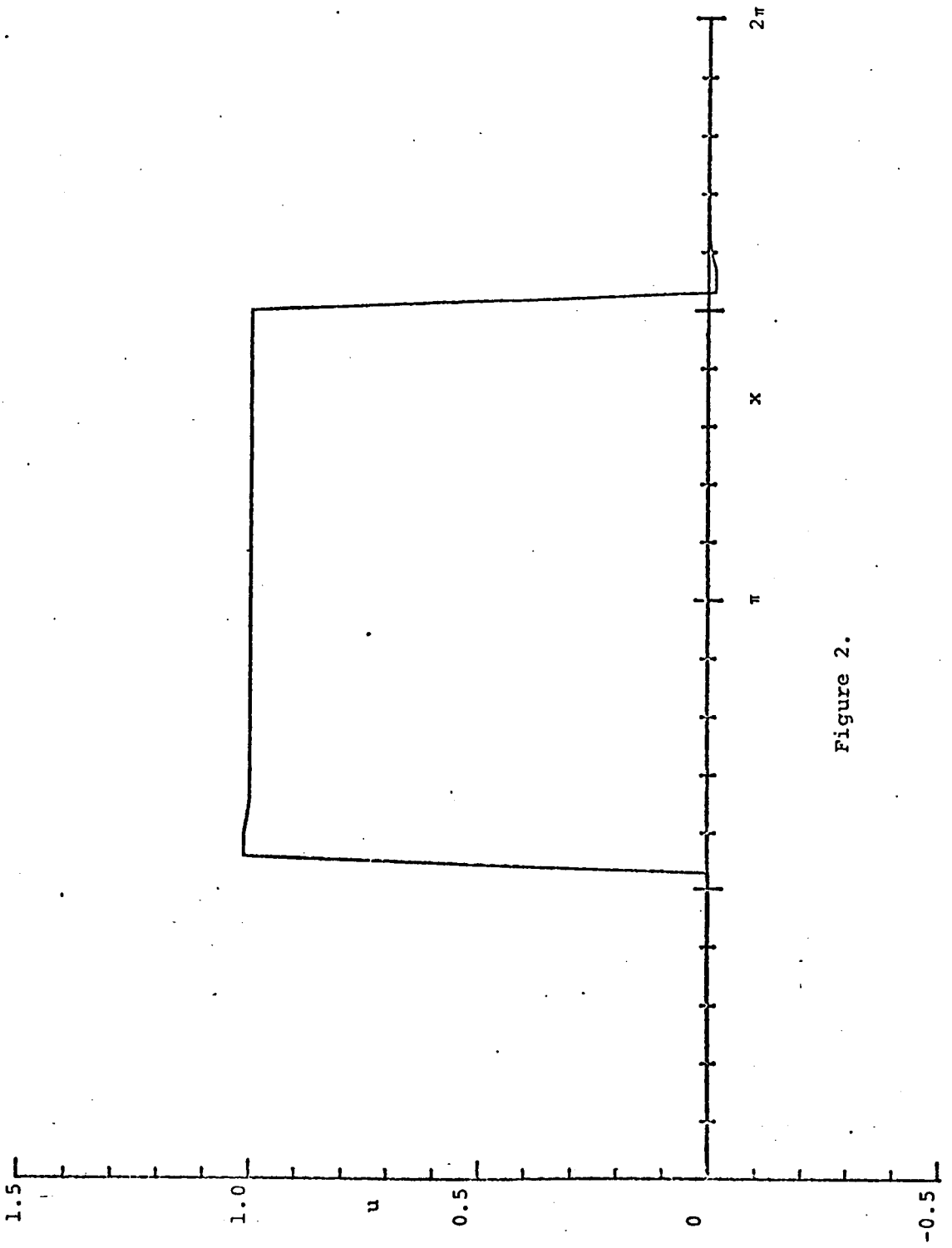

Figure 2.

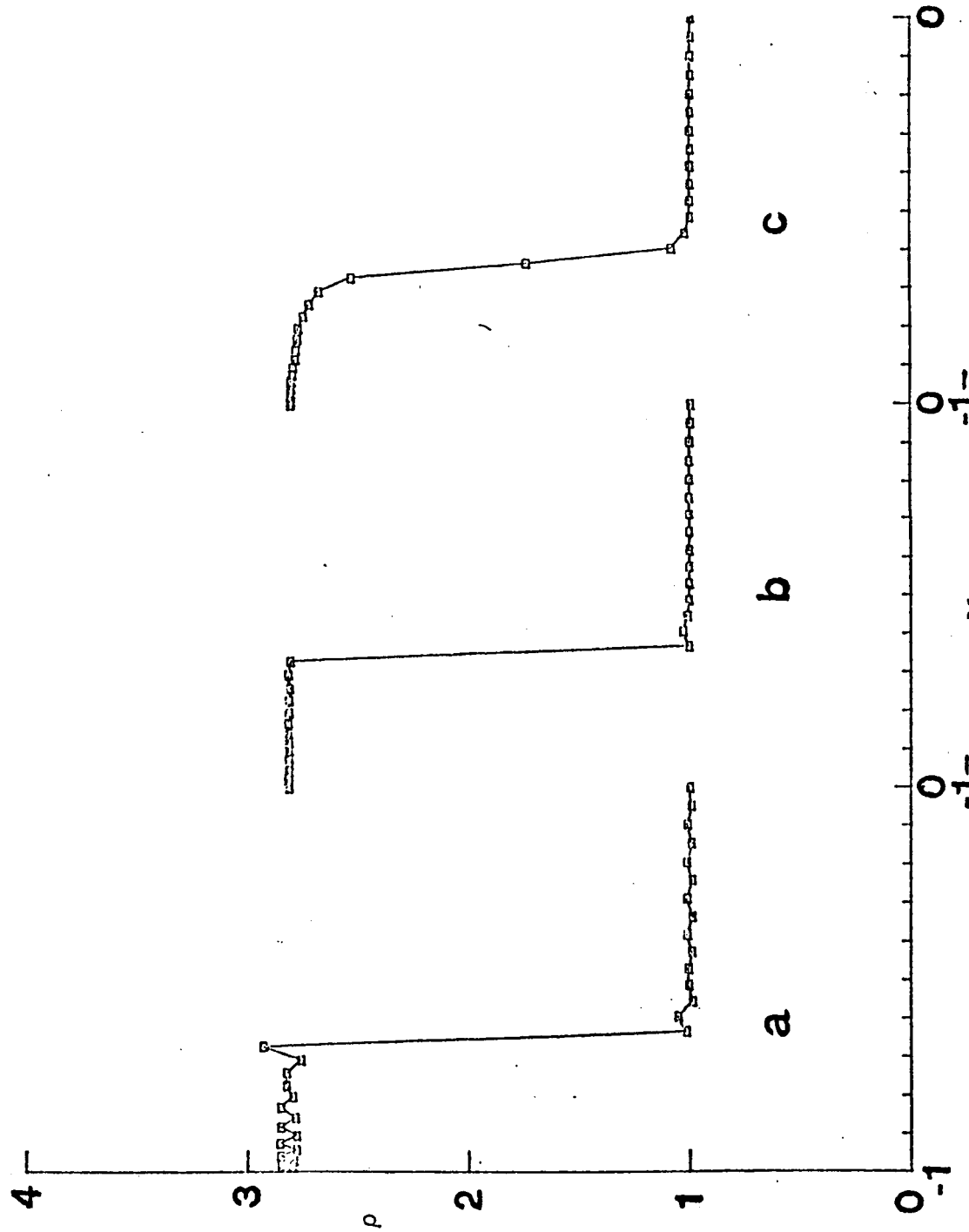

Figure 3.

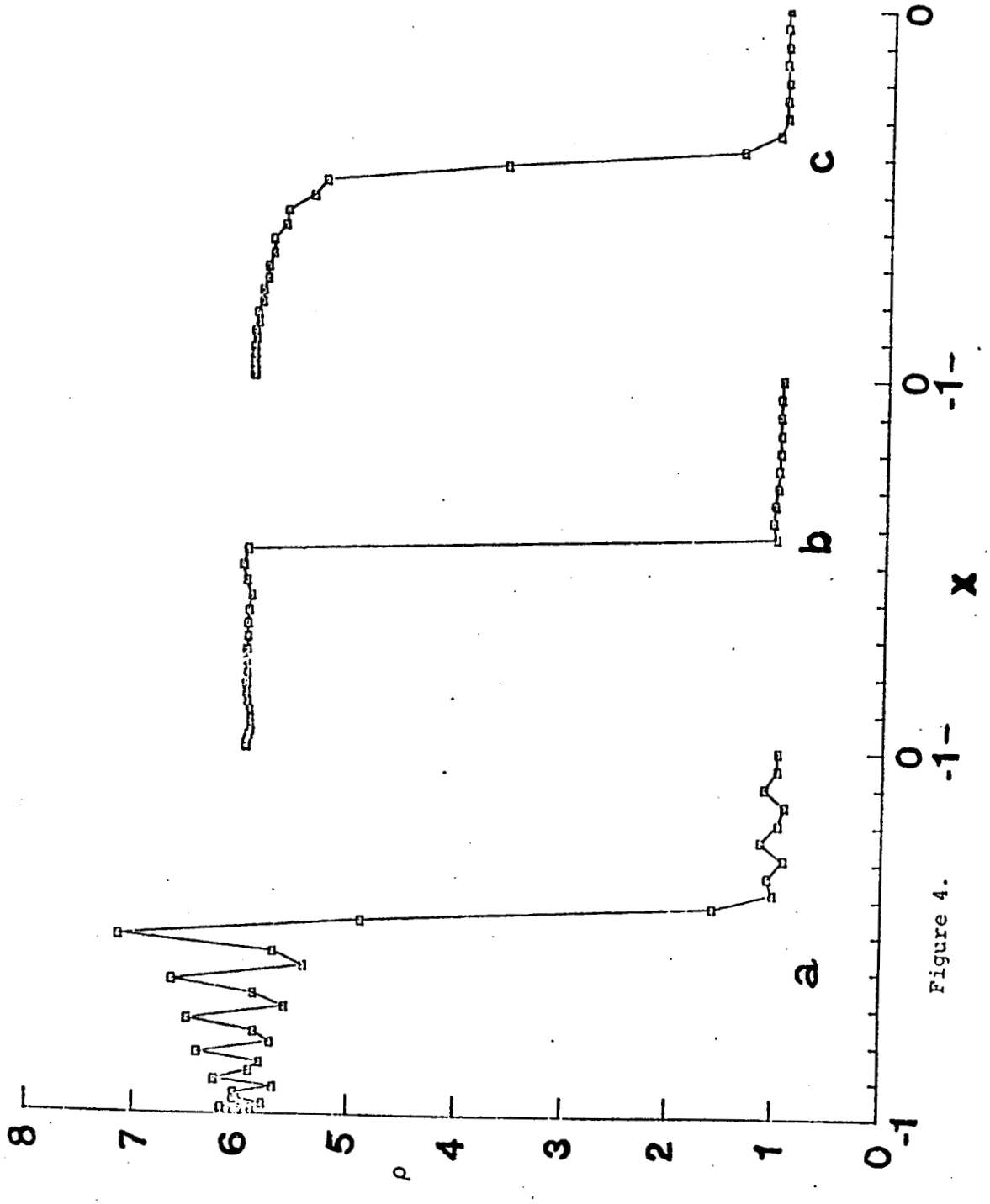

Figure 4.

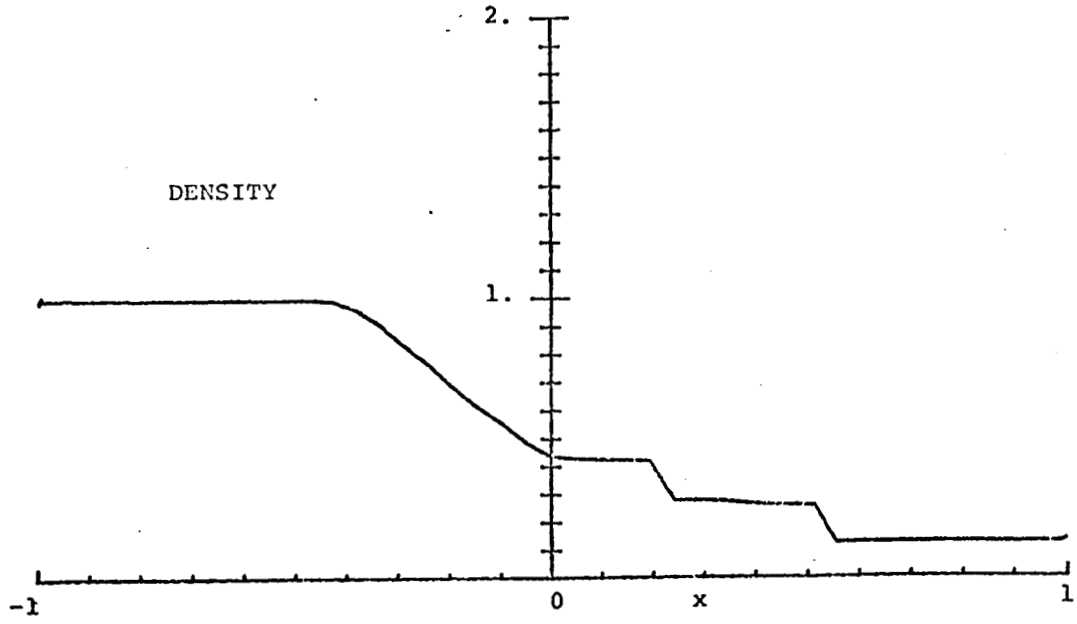

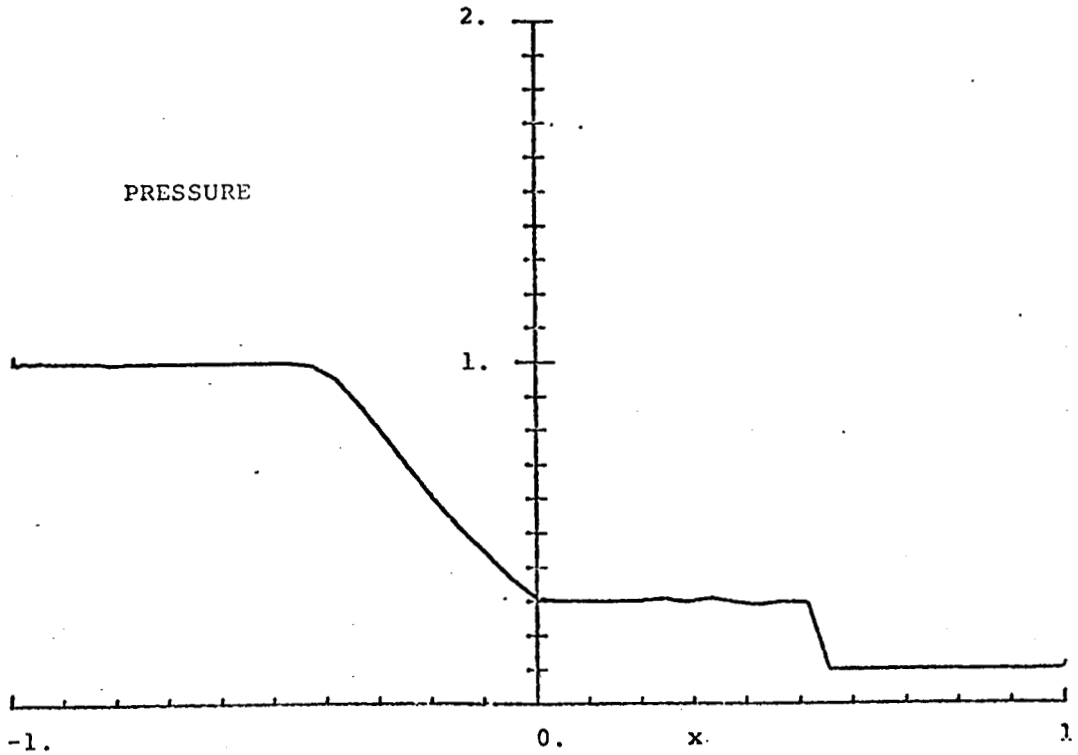

Figure 5.

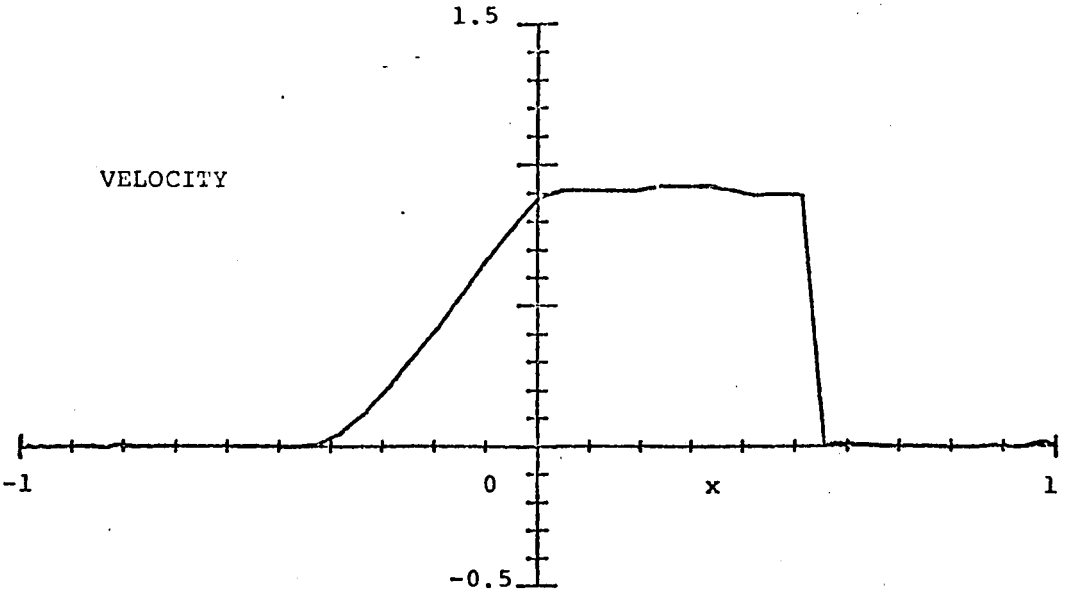

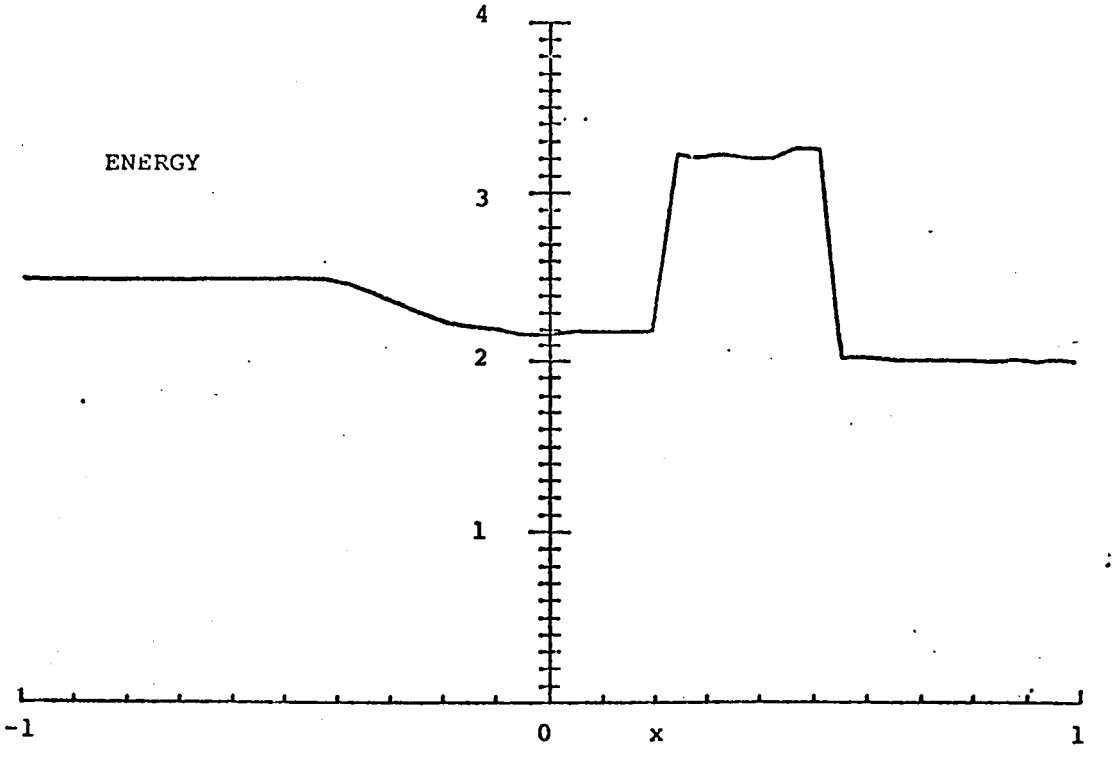

Figure 5 (cont'd).

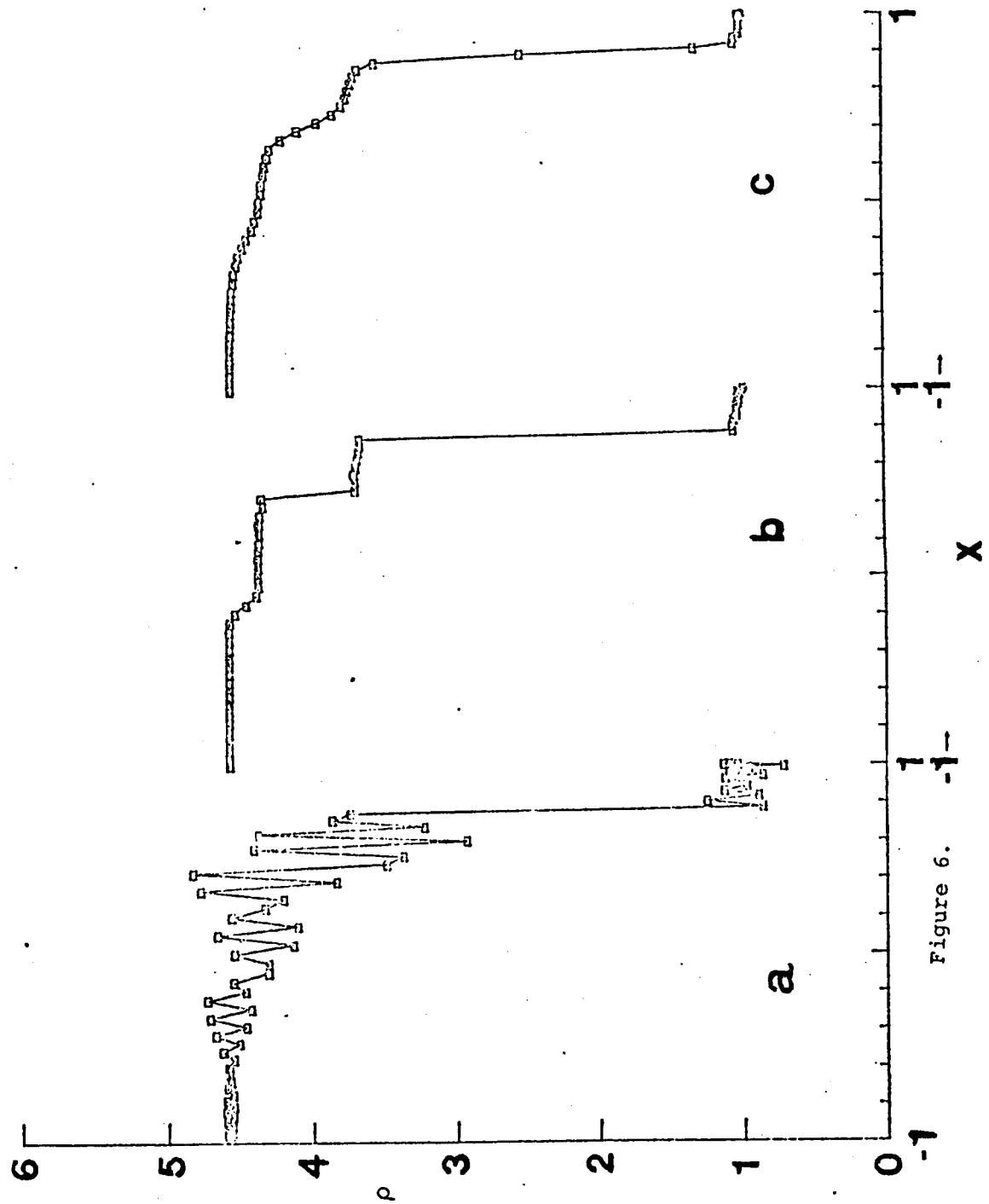

Figure 6.